frontiers | Frontiers in Cell Death

TYPE Original Research
PUBLISHED 14 November 2023
DOI 10.3389/fceld.2023.1182239

OPEN ACCESS

EDITED BY
Brett Williams,
Queensland University of Technology, Australia

REVIEWED BY
Haocai Chang,
South China Normal University, China
Haider H. Dar,
University of Pittsburgh, United States

*CORRESPONDENCE
Nils Helge Schebb,
nils@schebb-web.de
Dieter Steinhilber,
steinhilber@em.uni-frankfurt.de
Ann-Kathrin Häfner,
haefner@pharmchem.uni-frankfurt.de

RECEIVED 08 March 2023
ACCEPTED 23 October 2023
PUBLISHED 14 November 2023

CITATION
Goebel B, Carpanedo L, Reif S, Göbel T, Simonyi S, Schebb NH, Steinhilber D and Häfner A-K (2023), Development of a cell-based model system for the investigation of ferroptosis.
Front. Cell. Death 2:1182239.
doi: 10.3389/fceld.2023.1182239

Development of a cell-based model system for the investigation of ferroptosis

Bjarne Goebel[1], Laura Carpanedo[2], Susanne Reif[2], Tamara Göbel[1], Svenja Simonyi[1], Nils Helge Schebb[2]*, Dieter Steinhilber[1]* and Ann-Kathrin Häfner[1]*

[1]Institute of Pharmaceutical Chemistry, Goethe University Frankfurt, Frankfurt am Main, Germany, [2]Chair of Food Chemistry, Faculty of Mathematics and Natural Sciences, University of Wuppertal, Wuppertal, Germany

Since 2005, the original three cell death mechanisms apoptosis, autophagy and necrosis are accompanied by several new forms. The most recent member, ferroptosis, was first described in 2012 and is characterized by the accumulation of iron and increased lipid peroxidation. In this study, we present a model system to study ferroptotic states in stably transfected HEK293T cells, using acyl-CoA synthetase long chain family member 4 (ACSL4), a biomarker of ferroptosis, and/or lysophosphatidylcholine acyltransferase 2 (LPCAT2), a transferase responsible for the lipid remodeling process. In addition, we introduced an inducible expression system for 5-lipoxygenase (LO), 15-LO1 and 15-LO2, to trigger enzymatic lipid peroxidation. We characterized the system in terms of ACSL4, LPCAT2 and LO expression both on Western blot level and by laser scanning confocal microscopy as well as the intracellular localization of all enzymes. Furthermore, we verified inducibility and activity of our LOs and, in addition, analyzed non-esterified (free) and total amounts of oxylipins. When cells were incubated with the ferroptosis-inducing agents GPX4 inhibitor RSL3 or GSH reducing erastin, we observed a decrease in cell viability that was strongly enhanced in the presence of ACSL4 and LPCAT2. Interestingly, additional expression of LPCAT2 resulted in altered localization of 15-LO1, which shifted from the cytosol to the nuclear membrane. A similar localization occurred after treatment with RSL3. Therefore, on one hand, we propose that LPCAT2 is an acyltransferase that promotes ferroptotic conditions, and on the other hand, we introduce a new cell-based model system suitable for studying ferroptosis.

KEYWORDS

cell death, ferroptosis, ACSL4, LPCAT2, lipoxygenase, oxylipins, LC-MS, immunofluorescence

1 Introduction

In addition to the well-established types of cell death, the so-called programmed cell death or apoptosis, the cell death by autophagy and finally necrosis as a consequence of severe cell damage caused by physical, mechanical or chemical causes, novel forms of regulated cell death (RCD) such as necroptosis, pyroptosis or NETosis have been discovered and expanded our understanding of RCD. 10 years ago, one special type of RCD was uncovered and named ferroptosis, a new iron-dependent form of cell death. Characteristic

for this kind of cell death is the accumulation of non-heme iron and oxidative stress due to glutathione depletion (Dixon et al., 2012) which leads to lipid peroxidation (Chen et al., 2021b). While lipid peroxidation can occur through iron-mediated ROS production, known as Fenton reaction (Chen et al., 2020), it is also mediated through iron-containing enzymes like cytochrome P450 oxidoreductase (Zou et al., 2020; Yan et al., 2021) and lipoxygenases (LOs) (Yang et al., 2016; Wenzel et al., 2017; Kuang et al., 2021; Li et al., 2021) whose products, hydro(pero) xylated polyunsaturated fatty acids (PUFAs) also referred to as oxylipins, were shown to sensitize cells to ferroptosis (Shah et al., 2018). An insertional mutagenesis approach revealed that, among others, acyl-CoA synthetase long chain family member 4 (ACSL4), an enzyme necessary for the activation of fatty acids, and lysophosphatidylcholine acyltransferase 3 (LPCAT3), an enzyme required for membrane remodeling, are linked to ferroptosis (Dixon et al., 2015). ACSL4 which was later proposed as a biomarker for ferroptosis (Yuan et al., 2016), is expressed in the adrenal gland, ovary, testis and brain (Kang et al., 1997) and associated with endosomes, peroxisomes, as well as plasma, ER and mitochondrial membranes (Lewin et al., 2001; Küch et al., 2014; Liu et al., 2014; Ansari et al., 2017). ATP-dependent activation of fatty acids is a two-step reaction that results in the formation of an acyl-AMP intermediate, the AMP portion of which is subsequently substituted by coenzyme A (CoA). The resulting activated fatty acid is an acyl-CoA thioester that serves as substrate for phospholipid acyltransferases. LPCAT3 belongs to the lysophosphatidylcholine acyltransferase family and is one of four LPCATs involved in the process of lipid remodeling known as Lands' cycle (Lands, 1958; Wang and Tontonoz, 2019). Here, *sn*-2 fatty acyl moieties are released from phospholipids by phospholipase A2-mediated hydrolysis, resulting in 1-acyl lysophospholipids. Subsequently, the activated acyl-CoAs, mainly polyunsaturated fatty acid CoAs, can be incorporated into the membrane to form intact phospholipids (Lands and Merkl, 1963). This highlights the importance of LPCAT-mediated lipid remodeling in the context of increased lipid oxidation during ferroptosis. Over the years, several studies addressed the importance of ferroptosis. It has been shown to play a role in tumor suppression (Jiang et al., 2015; Chu et al., 2019) and aging (Stockwell, 2022), but is also associated with iron overload diseases (Wang et al., 2017), infections (Dar et al., 2018; Amaral et al., 2019; Yamane et al., 2022), and autoimmune disorders (Lai et al., 2022).

In 2021, Chen et al. (2021a) summarized these findings in a review article and postulated that macrophage polarization could also be influenced by ferroptosis and *vice versa*. Macrophages are responsible for the maintenance of tissue homeostasis, which includes the removal of ferroptotic cells (Luo et al., 2021). Of note, ferroptosis also seems to modulate macrophage polarization (Han et al., 2021).

Regarding the lipid modulating enzymes involved in ferroptosis, macrophages not only express ACSL4 but also high levels of LPCAT2, an isoenzyme of the commonly observed LPCAT3 (Shindou et al., 2007). The enzyme, also known as AGPAT11 (Agarwal and Garg, 2010), lysoPAFAT (Shindou et al., 2007) and AYTL1 (Soupene et al., 2008), is capable of transferring both acetyl and longer acyl chains from CoA-linked thioesters into lysophospholipids, preferably LPC (Shindou et al., 2007) and thus accepts a wider range of substrates compared to LPCAT3. While LPCAT2 and LPCAT3 are both expressed in the ER membrane, LPCAT2 is also found in lipid droplets (Wang and Tontonoz, 2019). The product spectrum of LPCAT2 includes 2-*O*-alkyl-PC known as platelet-activating factor (PAF) as well as 1-*O*-alkyl-PC (Shindou et al., 2007). Since PAF is an important factor and biomarker for various allergic and non-allergic inflammatory diseases such as asthma, psoriasis and ovarian cancer (Upton et al., 2022), it is obvious that LPCAT2 plays a role in the context of inflammatory diseases. Moreover, LPCAT2 mRNA expression was upregulated after macrophage treatment with TLR2, -4 or -9 ligands (Shindou et al., 2007; Abate et al., 2020) further underlining its importance in regulating inflammation.

Even though both LPCAT enzymes show a similar cellular localization and are involved in the Lands' cycle, only LPCAT3 has been studied in the context of ferroptosis so far. In order to investigate the role of LPCAT2 in the context of ferroptosis, we established a HEK293T-based model system in which LPCAT2 and/or ACSL4 are stably overexpressed. In addition, cells were equipped with doxycycline-inducible 5-LO, 15-LO1 or 15-LO2 to increase the ferroptotic burden in a controlled manner. With this model, the effects of LPCAT2 and the different lipoxygenases as well as various ferroptotic conditions on free oxylipins and the oxylipin composition of cellular membranes can be studied.

2 Material and methods

2.1 Cell culture

If not stated otherwise, reagents for cell culture use were obtained from Thermo Fisher Scientific™ (Waltham, Massachusetts, United States) or their associated company Life Technologies™ (Carlsbad, California, United States). Human embryonic kidney 293T cells (HEK293T, DSMZ, ACC 635, RRID: CVCL_0063, Braunschweig, Germany) and their genetically modified cell clones were cultured in Dulbecco's Modified Eagle Medium (DMEM) supplemented with 10% (v/v) FCS, 100 U/mL penicillin, 100 µg/mL streptomycin and 1 mM sodium pyruvate (culture medium, CM) in a humidified atmosphere with 5% CO_2 at 37°C.

Human monocytes were purified from peripheral blood mononuclear cells (PBMCs) isolated from leukocyte concentrates (DRK blood donor service, Frankfurt am Main, Germany). Donors gave written consent for use in research. After PBMC isolation through density gradient centrifugation as described elsewhere (Ebert et al., 2020), PBMCs were washed and resuspended in 40 mL wash medium (RPMI 1640 with 100 U/mL penicillin and 100 µg/mL streptomycin) per donor. The cell suspension was seeded to 10 cm^2 Petri dishes (8 dishes per donor; TC Dish 100 Cell+ 100 × 20 mm, for challenging adherent cells, SARSTEDT AG and Co., Nümbrecht, Germany) and left to adhere for 2 h at 37°C and 5% CO_2. Afterwards, adherent monocytes were washed twice using warm wash medium. Subsequently, cells were overlaid with complete growth medium (RPMI 1640 with 5% human serum, 100 U/mL penicillin and 100 µg/mL streptomycin) supplemented with either GM-CSF (10 ng/mL for M1 macrophages, PeproTech) or

M-CSF (10 ng/mL for M2 macrophages, PeproTech) and cultured for 7 days. Medium was renewed every other day. Within the last 48 h of differentiation, cells were additionally treated with INFγ (10 ng/mL for M1 macrophages, PeproTech) or IL-4 (10 ng/mL for M2 macrophages, PeproTech).

2.2 Plasmid preparation

pSBbiGH (RRID: Addgene_60514) and pSBtetGP (RRID: Addgene_60495) were a gift from Eric Kowarz. Human cDNA clones of '*Homo sapiens* acyl-CoA synthetase long-chain family member 4' (ACSL4) and '*Homo sapiens* lysophosphatidylcholine acyltransferase 2' (LPCAT2) were purchased from BioCat GmbH, Heidelberg, Germany.

Plasmids for stable transfection were prepared based on the optimized sleeping beauty (SB) system described by Kowarz et al. (2015). Constitutive protein expression constructs were prepared by exchanging the firefly luciferase in the MCS of pSBbiGH with the gene of interest (ACSL4 (short isoform), LPCAT2 or ACSL4 and LPCAT2 separated by P2A linker). For doxycycline-dependent expression of lipoxygenases, the GFP sequence of pSBtetGP inducible vector was exchanged to mCherry, before the gene of interest (*ALOX5*, *ALOX15* or *ALOX15B*) was inserted into the MCS. Constructs were prepared via common restriction cloning (SfiI: pSBbiGH_ACSL4, pSBbiGH_LPCAT2, pSBtetmChP_15LO1, pSBtetmChP_15LO2) or by restriction free cloning (pSBbiGH_ACSL4+LPCAT2, pSBtetmChP, pSBtetmChP_5LO) using the NEBuilder® HiFi DNA Assembly Master Mix according to the manufacturer's protocol (restriction enzyme and master mix were purchased from New England Biolabs Inc., Ipswich Massachusetts, United States).

2.3 Generation of stable cell lines

For each construct 0.1×10^6 cells were seeded into 6-well microplates. After 24 h the medium was changed to 2 mL fresh CM per well. Then, stable transfection was performed for 16 h using polyethyleneimine (PEI, branched, average MW 25,000 Da, Sigma-Aldrich) in a DNA to PEI ratio of 1:5. All DNA mixes contained a SB plasmid and the 100X transposase plasmid (kindly provided by Zoltan Ivics, Paul-Ehrlich-Institut, Langen, Germany) in a ratio of 9:1 (2.5 µg total DNA). After this, the medium was exchanged to fresh CM. After another 24 h, antibiotic selection of the stably transfected cells was initiated by using either 400 µg/mL hygromycin B or 2.5 µg/mL puromycin, until all cells showed the respective fluorescence (green for constitutive constructs and red for inducible constructs). During this period, the antibiotic containing medium was replaced every day.

2.4 Western blot analysis

For analysis of protein expression, inducible HEK293T cell lines were cultured in CM containing 200 ng/mL doxycycline (Sigma-Aldrich) for 24 h prior to cell harvest. Control cells as well as stable cell lines transfected for constitutive protein expression were not treated. Pellets of 5×10^6 cells were resuspended in 100 µL lysis buffer (20 mM Tris, pH 7.4, 150 mM NaCl, 2 mM EDTA, 1% Triton X-100, 0.5% NP-40 supplemented with protease inhibitor cocktail and phosphatase inhibitor mix (cOmplete mini and PhosSTOP, respectively, Roche, Basel, Switzerland)). Cell suspensions were sonicated (3×10 s) using an ultrasonic homogenizer (Sonopuls HD 200 with Sonopuls microtip MS 72 at 10% of the maximum amplitude, BANDELIN electronic GmbH and Co. KG, Berlin, Germany) and centrifuged (10 min, 15,000 rcf, 4°C). Supernatants were transferred to fresh 1.5 mL tubes and protein concentrations were determined using the Pierce™ BCA Protein Assay Kit (Thermo Fisher Scientific™). Total protein amounts (20–40 µg) per lysate were separated by SDS-PAGE using Precision Plus Protein™ All Blue Prestained Protein Standards as reference (Bio-Rad, Hercules, California, United States) and blotted onto nitrocellulose membranes (0.2 µm, Bio-Rad) using wet tank blotting or by semi dry method using the Trans-Blot Turbo transfer system (Bio-Rad). Protein expression was analyzed using primary antibodies listed in Table 1. GAPDH or ß-actin expression was used as loading-control. IR dye-coupled secondary antibodies (IRDye-680RD Anti-Goat IgG, IRDye 800CW Anti-Goat IgG, IRDye-680RD Anti-Mouse IgG, IRDye 800CW Anti-Mouse IgG, IRDye 800CW Anti-Rabbit IgG, LI-COR Biosciences, Bad Homburg, Germany) were used to visualize antibody-protein complexes and immune reactive bands were imaged on an Odyssey infrared imaging system (LI-COR Biosciences).

2.5 Determination of lipoxygenase product formation

Product formation of lipoxygenases was analyzed as described recently (Kreiß et al., 2022). In brief, 5×10^6 cells were seeded per 15 cm dish. After cell adherence for 24 h, lipoxygenase expression was induced by treatment using 200 ng/mL doxycycline with untreated cells as control. After 24 h, cells were harvested with TE (trypsin EDTA, Thermo Fisher Scientific™), washed with 5 mL PBS and resuspended in PGC buffer (PBS containing 1 mg/mL α-D-glucose and 1 mM $CaCl_2$) in a final concentration of 5×10^6 cells/mL. The reaction was started by addition of 20 µM arachidonic acid (AA, Cayman Chemical Company) and 2.5 µM calcium ionophore A23187 (Sigma-Aldrich). Reaction was stopped after 10 min at 37°C by addition of 1 mL ice cold methanol (LC-MS grade, Carl Roth®, Karlsruhe, Germany). Afterwards, sample preparation (Werz and Steinhilber, 1996) and product analysis by means of LC-UV (Kreiß et al., 2022) were performed as described previously. In addition, 12-HETE and 15-HETE were analyzed at 235 nm and 319.2 Da.

2.6 Immunohistochemistry

2×10^4 cells/well (with inducible lipoxygenase expression) were seeded into 8-well Nunc™ Lab-Tek™ II CC2™ chamber slides (Thermo Fisher Scientific™), and were left to adhere for 24 h. Then, lipoxygenase expression was induced by treatment with 200 ng/mL doxycycline for 24 h. Cells were treated with 10 µM RSL3 or 3 µM erastin (Sigma-Aldrich) for 4 h or 24 h, respectively, while DMSO treated cells served as control. Cells were carefully

TABLE 1 Primary antibodies used for Western blot analysis.

Target	RRID	Species	Dilution	Supplier
15-LO1 (ab119774)	AB_10901109	Mouse	1:2,000	Abcam, Cambridge, United Kingdom
15-LO2 (sc-271290)	AB_10609897	Mouse	1:500	Santa Cruz Biotechnology, Dallas, Texas, United States
5-LO (sc-515821)	no RRID entry	Mouse	1:500	Santa Cruz Biotechnology
ACSL4 (sc-365230)	AB_10843105	Mouse	1:100	Santa Cruz Biotechnology
FSP1 (sc-377120)	AB_2893240	Mouse	1:200	Santa Cruz Biotechnology
GAPDH (#2118)	AB_561053	Rabbit	1:1,000	Cell Signaling Technology, Danvers, Massachusetts, United States
GPX4 (sc-50497)	AB_1124979	Rabbit	1:100	Santa Cruz Biotechnology
LPCAT2 (PA5-39008)	AB_2555600	Rabbit	1:1,000	Thermo Fisher Scientific™, Waltham Massachusetts, United States
LPCAT3 (MAG531Hu21)	no RRID entry	Mouse	1:1,000	Cloud-Clone Corp., Houston, Texas, United States
ß-actin (ab8229)	AB_306374	Goat	1:1,000	Abcam

TABLE 2 Antibody dilutions for laser scanning confocal microscopy analysis.

Target	Dilution
5-LO (10021-1-Ig, Proteintech, RRID: AB_513237, Rosemont, Illinois, United States)	1:50
5-LO (66326-1-lg, Proteintech, RRID: AB_2881707)	1:50
15-LO1 (ab119774, RRID: AB_10901109)	1:50-100
15-LO2 (sc-271290, RRID: AB_10609897)	1:50-100
ACSL4 (sc-365230, RRID: AB_10843105)	1:50
LPCAT2 (PA5-39008, RRID: AB_2555600)	1:50

washed with cold PBS and fixated using 4% PFA in PBS for 15 min at RT. Slides were washed twice (PBS) and permeabilization and blocking was performed for 1 h at RT with 1% (w/v) BSA, 0.2% (v/v) Triton X-100 and 22.54 mg/mL glycine in PBS. Primary antibody incubations were performed either overnight at 4°C or for 3 h at RT in PBS with 1% (w/v) BSA, 0.2% (v/v) Triton X-100 and the respective target antibody (Table 2). Slides were washed again (PBS, 3x) and secondary antibody solutions (1:1,000, donkey anti-mouse, donkey anti-rabbit, goat anti-rabbit IgG (H + L) Highly Cross-Adsorbed Secondary Antibody coupled to Alexa Fluor™ Plus 647 and Alexa Fluor™ 532 goat anti-mouse IgG (H + L), Thermo Fisher Scientific™) were added for 1 h at RT, light protected. Cells were washed (PBS, 3x) and nuclei were stained with 1 µg/mL DAPI (Thermo Fisher Scientific™) for 10 min at RT followed by another washing step (PBS, 3x). Samples were mounted with Mowiol mounting medium (Carl Roth®) and Menzel coverslips (Thermo Fisher Scientific™) according to the manufacturer's protocol and kept at RT overnight. Finally, slides were sealed with clear lacquer and stored at 4°C until analysis. Imaging of sample slides was performed on a Zeiss 780 AxioObserver.Z1 laser scanning confocal microscope (Carl Zeiss AG, Oberkochen, Germany) with Argon and He/Ne 633 nm lasers in combination with a Zeiss Plan-Apochromat 63x/1.4 NA oil lens. Excitation was performed with 405, 514 and 633 nm lasers in separated tracks and the same pinhole size was applied during all measurements. The line average was set to 8 and was used for each channel.

2.7 Cell viability

2.5×10^4 cells/well were seeded in a 96-well microplate. After adherence, cells were treated for 24 h with varying concentrations of erastin (1–10 µM) or 1*S*,3*R*-RSL3 (0.1–10 µM; RSL3, Sigma-Aldrich) before 10 µL WST-1 reagent (Sigma-Aldrich) was added for 2 h at 37°C. Absorbance at 450 nm and 690 nm was measured (Tecan infinite® M200, Tecan Trading AG, Männedorf, Switzerland) and cell viability was calculated as described by the manufacturers' protocol (compared to DMSO controls).

2.8 LC-MS analysis of total and non-esterified oxylipins

1×10^7 HEK293T cells (wild type and stably transfected) were seeded in 15 cm Petri dishes and were allowed to adhere for 24 h. Medium of inducible cell lines was changed to induction medium for 24 h. Cells were scraped in ice cold PBS, centrifuged (340 rcf, 4°C for 5 min), and the pellets were washed with 1 mL fresh PBS. Following another centrifugation step (340 rcf, 4°C, 5 min) the supernatant was discarded and dry pellets were stored at −80°C.

For RSL3 treated samples, cells were seeded as described above. After doxycycline treatment, 10 µM RSL3, 1 µM Fer-1 (Sigma-Aldrich) or DMSO were added for 4 h before dry pellets were prepared.

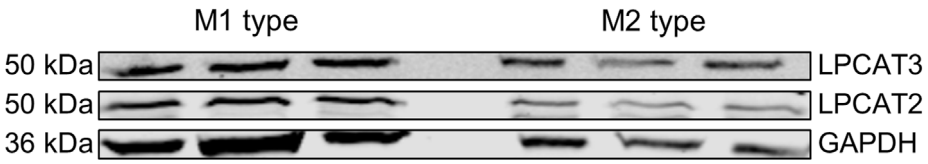

FIGURE 1
LPCAT2 and LPCAT3 expression in human monocyte-derived macrophages. Protein expression of LPCAT2 and LPCAT3 was analyzed by Western blot using GAPDH as loading control. M1 and M2 macrophages (20 µg/lane) were obtained after differentiation of monocytes from peripheral blood with 10 ng/mL GM-CSF or M-CSF for 7 days, respectively. 10 ng/mL IFNγ (M1) or 10 ng/mL IL-4 (M2) were added during the last 48 h of differentiation. Side-by-side bands (left: M1 type; right: M2 type) display three independent experiments.

The dry pellet was resuspended in 490 µL PBS or 490 µL H_2O/50% (*v/v*) methanol and 10 µL antioxidant mixture (10 µL 0.2 mg/mL butylated hydroxytoluene, 100 µM indomethacin, 100 µM soluble epoxide hydrolase inhibitor *trans*-4-[4-(3-adamantan-1-yl-ureido)-cyclohexyloxy]-benzoic acid and 500 µM 15-LO Inhibitor BLX3887) was added. Samples were vortexed and sonicated for 10 s. Hydroperoxides contained in sonicated cells were reduced to corresponding alcohols by addition of 5 mM $SnCl_2$ for 10 min at RT (10 mg/mL $SnCl_2$ solution in MeOH). Non-esterified and total oxylipins were prepared and analyzed by LC-MS following solid phase extraction as described (Rund et al., 2018; Kutzner et al., 2019; Ostermann et al., 2020; Hartung et al., 2023).

2.9 Statistical analysis

Data are presented as mean + standard deviation (SD) of three independent experiments. Statistical analysis was performed using 2-way ANOVA with Dunnett's multiple comparisons test. $^{*}p < 0.05$, $^{**}p < 0.01$, $^{***}p < 0.001$. Significance was determined using GraphPad Prism7 (GraphPad Software, San Diego, California, United States).

3 Results

3.1 LPCAT2 and LPCAT3 expression in human primary macrophages

Macrophages are responsible for the clearance of malfunctioning cells and cellular debris which includes ferroptotic cells (Luo et al., 2021). Thereby, the risk of developing ferroptosis themselves is increased. In addition, this risk is further enhanced due to high expression levels of the pro-ferroptotic enzymes ACSL4, an enzyme considered crucial for the development of ferroptosis (Doll et al., 2017) and the presence of LPCAT3, a member of the lysophospholipid acyltransferase family involved in lipid remodeling. Interestingly, macrophages are also described to contain high protein levels of LPCAT2, an isoenzyme of LPCAT3, which is known to accept a broad range of substrates (Yamashita et al., 2014) and in contrast to LPCAT3, has not been studied in the context of ferroptosis so far (Shindou et al., 2007). Thus, we wondered whether LPCAT2 might also be involved in the context of ferroptosis. According to the human protein atlas database the RNA expression of LPCAT2 (97.3 nTPM; normalized transcripts per million) in macrophages is 6-times higher compared to LPCAT3 (15.8 nTPM). Consequently, we checked the protein expression of LPCAT2 and LPCAT3 in human primary monocyte-derived macrophages types M1 and M2 on Western blot (Figure 1) and confirmed that both enzymes are strongly expressed in human macrophages. Therefore, we decided to further investigate the role of LPCAT2 in ferroptosis by establishing a robust and easy to transfect HEK293T based stable overexpression system of LPCAT2 together with the ferroptosis promoting enzyme ACSL4 and various lipoxygenases.

3.2 Generation of HEK293T cells stably overexpressing LPCAT2 with or without ACSL4 and inducible expression of various lipoxygenases

We prepared HEK293T cell lines stably overexpressing the human ACSL4 gene, and/or the human LPCAT2 gene, (HEK293T_ACSL4, HEK293T_LPCAT2 and HEK293T_A+L, respectively), together with an empty vector control cell line (HEK293T_VC) using an optimized sleeping beauty system followed by antibiotic selection. Expression of both enzymes was verified by immunoblotting (Figure 2). HEK293T cells already express endogenous ACSL4 detectable by Western blot. Overexpression of ACSL4 led to a 3-fold increase in ACSL4 levels in HEK293T_ACSL4 cells and about 2.5-fold in HEK293T_A+L cells. In contrast, HEK293T_LPCAT2 cells showed a small decrease in endogenous ACSL4 levels compared to vector control cells (Figure 2A). For LPCAT2, basal expression in HEK293T cells is quite low and overexpression of the LPCAT2 gene resulted in a 13-fold increase in LPCAT2 levels in HEK293T_A+L cells and an even stronger increase of about 30-fold in HEK293T_LPCAT2 cells (Figure 2B). As expected, expression of ACSL4 and LPCAT2 was not altered in empty vector control cells compared to HEK293T wild type cells. To further mimic the oxidative conditions in ferroptotic cells, we additionally transfected the cells with either doxycycline-inducible 5-lipoxygenase (LO), 15-LO1 or 15-LO2 to increase lipid peroxidation. In order to prevent these cell lines from an unwanted early cell death, LO expression is silenced in the absence of doxycycline (Kowarz et al., 2015). As HEK293T cells already express detectable amounts of ACSL4 and based on an initial oxylipin screening (data not shown) we added the inducible LO expression to the three cell lines HEK293T_A+L, HEK293T_LPCAT2 and HEK293T_VC resulting in nine cell lines in total. Figure 2C shows LO expression

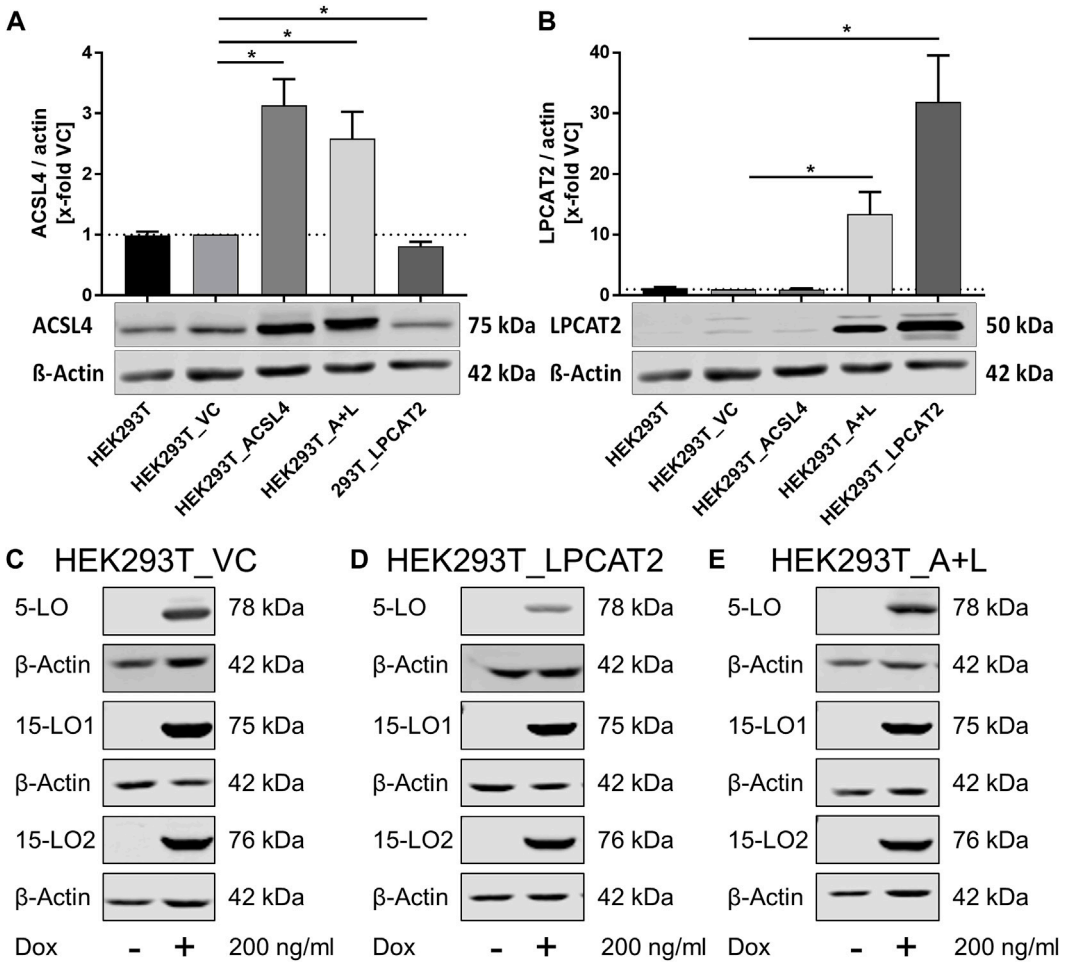

FIGURE 2
Protein expression in stably transfected HEK293T cells. Densitometric analysis of the protein expression of ACSL4 **(A)** and LPCAT2 **(B)** in HEK293T wild type and vector control cells (HEK293T_VC) and HEK293T stably overexpressing ACSL4 (HEK293T_ACSL4), LPCAT2 (HEK293T_LPCAT2) or ACSL4/LPCAT2 (HEK293T_A+L) by quantitative Western blot, using β-actin as loading control. **(C–E)** Inducible protein expression of 5-LO, 15-LO1 and 15-LO2 following doxycycline treatment (Dox, 200 ng/mL, 24 h) analyzed by Western blot. Each blot displays one different stable cell line derived from either HEK293T_VC **(C)**, HEK293T_LPCAT2 **(D)** or HEK293T_A+L **(E)**. **(A–E)** A representative blot is shown per experiment. **(A)+(B)**: Mean +SD of n = 3 experiments. Intensities were correlated to the housekeeping gene (β-actin) and normalized on the vector control cells. Statistical analysis: Unpaired *t*-test with Welch's correction against vector control. *$p < 0.05$.

in HEK293T_VC derived cells with 5-LO, 15-LO1 and 15-LO2 containing cells from top to bottom, respectively. LO expression was not detectable under standard culture conditions but clearly visible after doxycycline treatment (200 ng/mL, 24 h). HEK293T_LPCAT2 (Figure 2D) and HEK293T_A+L (Figure 2E) cells showed the same inducible LO expression confirming the functionality of the doxycycline-dependent expression system. Furthermore, expression of other ferroptosis related genes like FSP1 and GPX4 was not affected by LO induction (Supplementary Figure S1).

3.3 Analysis of LO product formation

Next, we addressed the LO activity in our inducible system. LOs are capable of converting multiple PUFAs (Figure 3) and we verified the enzymatic activity of our system using arachidonic acid (AA). Product formation was analyzed as described following stimulation with calcium ionophore A23187 and AA by means of LC-UV (Kreiß et al., 2022). Depending on the respective cell line, AA derived products of 5-LO (leukotriene B_4 (LTB_4), 6-*trans*-LTB_4, 6-*trans*-12-*epi*-LTB_4 and 5-HETE), 15-LO1 (12- and 15-HETE) and 15-LO2 (15-HETE) were detected and quantified (Figure 4). All cell lines showed comparable amounts of LO products following doxycycline treatment and as expected, no LO activity was found without induction resulting in a very robust and reliable cell-based model system to study ferroptosis.

3.4 Cellular localization of ACSL4 and LPCAT2

Next, we performed confocal laser scanning microscopy to check the cellular localization of ACSL4 and LPCAT2 after induction of LO expression (Figure 5). In accordance with our Western blot analyses (Figure 2) we could detect ACSL4 in all cell lines, regardless whether it

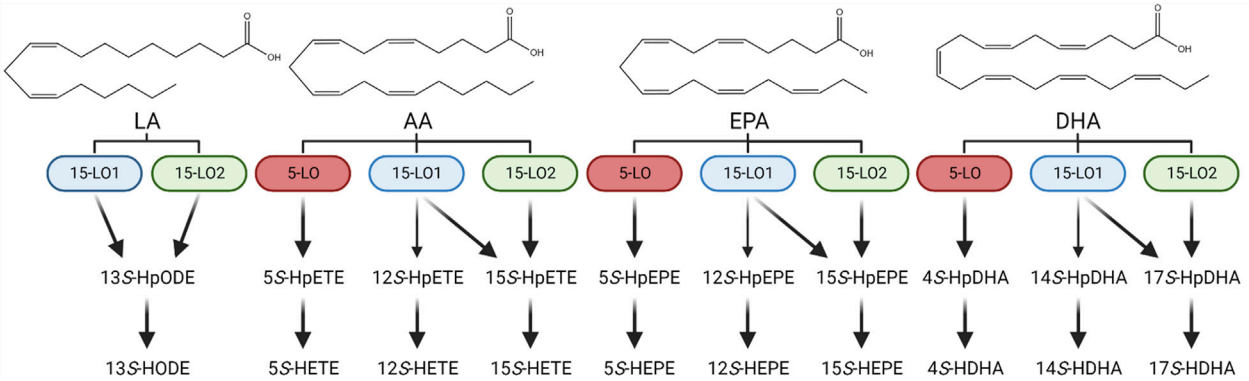

FIGURE 3
Enzymatic oxylipin formation scheme. Enzymatic conversion of linoleic acid (LA), arachidonic acid (AA), eicosapentaenoic acid (EPA) and docosahexaenoic acid (DHA) to their respective monohydroxylated oxylipins: 13*S*-HODE: 13*S*-hydroxy-9Z,11E-octadecadienoic acid; 5*S*-HETE: 5*S*-hydroxy-6E,8Z,11Z,14Z-eicosatetraenoic acid; 12*S*-HETE: 12*S*-hydroxy-5Z,8Z,10E,14Z-eicosatetraenoic acid; 15*S*-HETE: 15*S*-hydroxy-5Z,8Z,11Z,13E-eicosatetraenoic acid; 5*S*-HEPE: 5*S*-hydroxy-6E,8Z,11Z,14Z,17Z-eicosapentaenoic acid, 12*S*-HEPE: 12*S*-hydroxy-5Z,8Z,10E,14Z,17Z-eicosapentaenoic acid; 15*S*-HEPE: 15*S*-hydroxy-5Z,8Z,11Z,13E,17Z-eicosapentaenoic acid; 4*S*-HDHA: 4*S*-hydroxy-5E,7Z,10Z,13Z,16Z,19Z-docosahexaenoic acid; 14*S*-HDHA: 14*S*-hydroxy-4Z,7Z,10Z,12E,16Z,19Z-docosahexaenoic acid; 17*S*-HDHA: 17*S*-hydroxy-4Z,7Z,10Z,13Z,15E,19Z-docosahexaenoic acid.

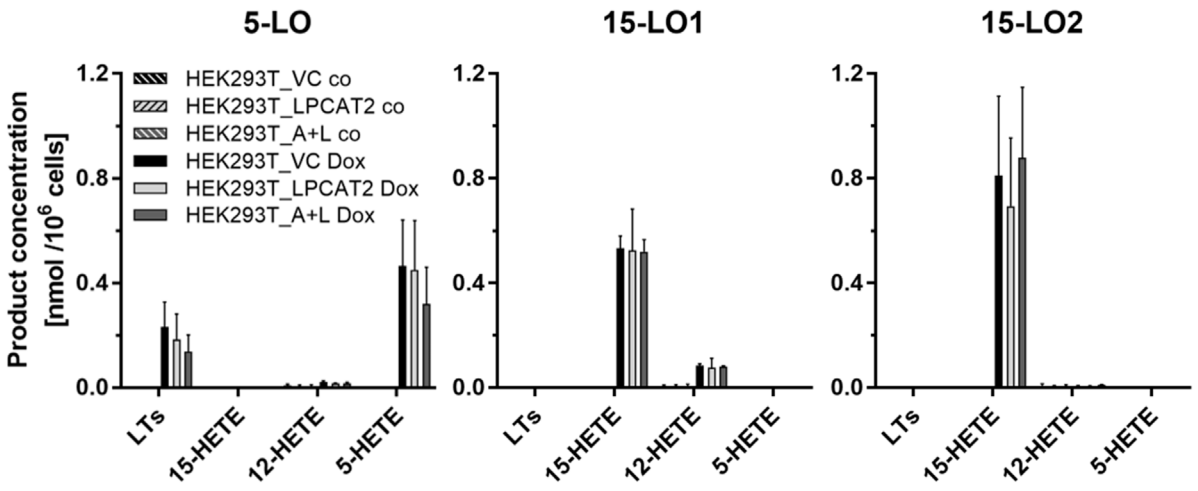

FIGURE 4
LO product formation in transfected HEK293T cells. LO product formation was analyzed in cells with (HEK293T_LPCAT2_LO, HEK293T_A+L_LO) or without (HEK293T_VC_LO) stable overexpression of LPCAT2 and LPCAT2/ACSL4 and inducible expression of either 5-LO, 15-LO1 or 15-LO2. For LO expression, cells were treated with (plain bars) or without (hatched bars) 200 ng/mL doxycycline for 24 h. Afterwards, 5 × 10^6 cells were stimulated by 20 µM AA, 2.5 µM calcium ionophore A23187 and 1 mM $CaCl_2$ for 10 min at 37°C and products were analyzed by LC-UV. Data were normalized on 10^6 cells (mean +SD, n = 3). Leukotrienes (LTs): 6-*trans*-LTB_4, 6-*trans*-12-*epi*-LTB_4 and LTB_4.

was overexpressed or not (see Supplementary Figure S2 for HEK293T_A+L cells). Additionally, ACSL4 is located exclusively in the cytosol of our cells. Therefore, we restricted our investigations via confocal microscopy on the cell lines HEK293T_LPCAT2 and HEK293T_VC. In contrast, the localization of LPCAT2 differed between overexpressing and vector control cells. In HEK293T_LPCAT2 cells, LPCAT2 expression was uniformly cytosolic, while small circular spots were observed in addition in HEK293T_VC cells. This is in line with current literature describing the localization of LPCAT2 as either associated with the ER membrane or included in lipid droplets (Wang and Tontonoz, 2019) which seems to be the case here. Furthermore, a difference in location of ACSL4 and LPCAT2 was not observed between 5-LO, 15-LO1 and 15-LO2 overexpressing cells. (Figure 5).

3.5 Ferroptosis inducing agents erastin and RSL3 show a cell line-dependent decrease in cell viability

Following the initial characterization of our LPCAT2 and ACSL4 overexpression system, we investigated the behavior

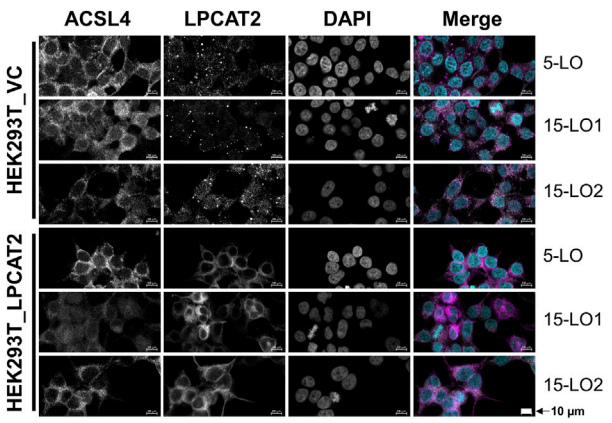

FIGURE 5
Localization of ACSL4 and LPCAT2 in stably transfected HEK293T cells. HEK293T_VC_LO and HEK293T_LPCAT2_LO (LO: 5-LO, 15-LO1 or 15-LO2), induced with 200 ng/mL doxycycline for 24 h, were stained with fluorophore-conjugated secondary antibodies against specific primary antibodies. Nuclei were counterstained using DAPI. Cells were imaged and analyzed on a Zeiss 780 AxioObserver.Z1 laser scanning confocal microscope (Carl Zeiss AG). Images display a representative part of the acquired total image. Fluorescence of single channels is shown in black and white for better contrast, with the overlaid image shown in color (ACSL4: white; LPCAT2: purple, DAPI: turquoise). 10 µm scale bars are given in each image. Brightness and contrast were adjusted in a linear fashion. Images display one of 3 independent experiments.

under ferroptotic conditions. To validate the system regarding its response to ferroptosis inducing agents, cell viability was tested using a WST-1 assay upon incubation with the two different ferroptotic inducers erastin (inhibitor of cystine/glutamate antiporter cXT) or RSL3 (GPX4 inhibitor). Both compounds showed a concentration-dependent decrease in cell viability (Figure 6) although the effect of erastin was stronger at the same concentration. HEK293T_VC cells did not appear to be affected at concentrations below 1 µM erastin and 3 µM RLS3. LPCAT2 containing cell lines however responded to the treatment even at lowest concentrations, indicating that the enzyme somehow promotes ferroptotic conditions. Comparison of HEK293T_LPCAT2 and HEK293T_A+L cells also revealed that additional overexpression of ACSL4 leads to stronger effects at most of the concentrations (except for 1 µM RSL3) which emphasizes the importance of ACSL4 as a contributor of ferroptosis (Yuan et al., 2016).

3.6 LPCAT2 expression causes localization changes of 5-LO, 15-LO1 and 15-LO2

Based on our cell viability data we treated HEK293T_LPCAT2 and HEK293T_VC cells after induction of the respective LO with either 10 µM RSL3 for 4 h, 3 µM erastin (Era) for 24 h or DMSO and checked the cellular localization of 5-LO, 15-LO1 and 15-LO2, respectively (Figure 7; for separated channels see Supplementary Figures S3–S5 and S6 for merged images of HEK293T_A+L cells). As treatment with RSL3 for 24 h resulted in detachment of the cells during the preparation process, the incubation time had to be shortened to 4 h.

In untreated HEK293T_VC_LO cells, all three LOs reside entirely in the cytosol. After erastin treatment, they partially translocate into the nucleus. The same is true for RSL3 treatment of 5-LO and 15-LO2 expressing cells whereas RSL3 led to a complete translocation of 15-LO1 to the nuclear membrane. In contrast, 5-LO is already distributed throughout the cell in HEK293T_LPCAT2_5LO, with no further effects of RSL3 and erastin treatment. In HEK293T_LPCAT2_15LO1 cells, 15-LO1 is already completely located at the nuclear membrane, whether the cells were treated with RSL3/Era or not.

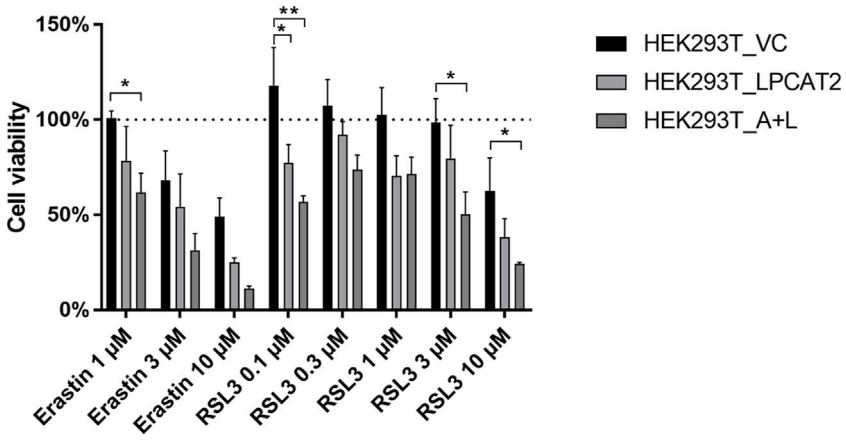

FIGURE 6
Effects of ferroptosis inducing agents on cell viability of stably transfected HEK293T cells. Cell viability was determined by WST-1 assay. 2.5 × 10^4 HEK293T_VC, HEK293T_LPCAT2 and HEK293T_A+L cells were treated with DMSO or indicated concentrations of ferroptosis inducers erastin or RSL3 for 24 h followed by treatment with 10 µL WST-1 reagent for 2 h at 37°C. Absorbance at 450 nm and 690 nm was measured on a Tecan infinite® M200 (Tecan Trading AG). Statistical analysis was performed against DMSO controls (100%) using 2-way ANOVA with Dunnett's multiple comparisons test (mean +SD, n = 3). *$p < 0.05$, **$p < 0.01$.

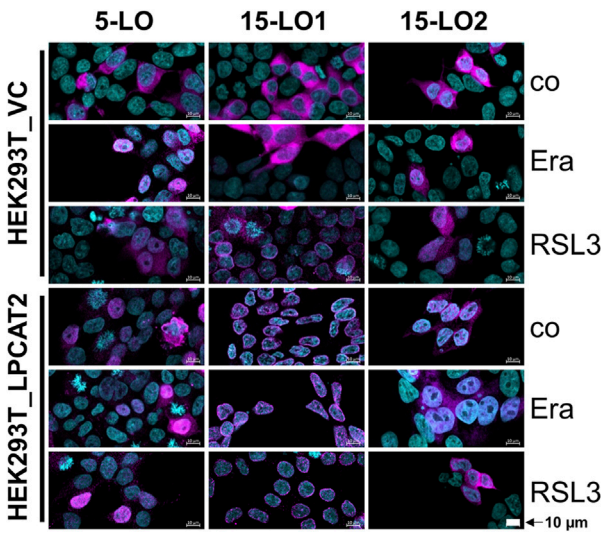

FIGURE 7
Effect of ferroptosis inducers on the localization of lipoxygenases in stably transfected HEK293T cells. HEK293T_VC_LO and HEK293T_LPCAT2_LO (left: 5-LO, center: 15-LO1, right: 15-LO2) cells were treated with 200 ng/mL doxycycline for 24 h before treatment with 10 µM RSL3 or 3 µM erastin (Era) for 4 or 24 h, respectively. Controls (co) received DMSO. Cells were stained with fluorophore-conjugated secondary antibodies against specific primary antibodies (LOs: purple). Nuclei were counterstained using DAPI (turquoise). Cells were imaged and analyzed on a Zeiss 780 AxioObserver.Z1 laser scanning confocal microscope (Carl Zeiss AG). Images display a representative part of the acquired total image. Overlaid images are shown with 10 µm scale bars. Brightness and contrast were adjusted in a linear fashion. Images display one of 3 independent experiments.

For 15-LO2, overexpression of LPCAT2 leads to a distribution throughout the cell, unaffected by erastin. In contrast, RSL3 promotes cytosolic localization of 15-LO2 in HEK293T_LPCAT2_15LO2 cells. To further investigate the correlation of LPCAT2 expression and cellular localization of all lipoxygenases, we performed stainings of both LPCAT2 and LOs in combination with RSL3 and erastin treatment in HEK293T_LPCAT2_LO cells (Figure 8A). In all three cell lines, LPCAT2 was mainly cytosolic and unaffected by RSL3 or erastin treatment. 5-LO and 15-LO2 were located in both nucleus and cytosol and their localization was also not affected by RSL3 or erastin treatment. 15-LO1 was located at the nuclear membrane and upon treatment with RSL3 and erastin distributed within the soluble part of the nucleus. As 15-LO1 was the only LO associated with the nuclear membrane we analyzed the intensities of each marker (purple: LPCAT2, white: 15-LO1, turquoise: DAPI) and correlated the data with the cellular profile (Figure 8B). Here, increased intensities of LPCAT2 and 15-LO1 at the nuclear membrane can be detected indicating a co-localization where a direct interaction of both enzymes might be possible.

3.7 RSL3 treatment increases oxylipin formation in HEK293T_LPCAT2_15LO1 cells

Finally, we investigated the effects of RSL3 or/and Ferrostatin-1 (Fer-1), a ferroptosis inhibitor, on the endogenous oxylipin formation in HEK293T_LPCAT2_LO cells (Figure 9). First, to get an impression of the oxylipin distribution in our cells, we analyzed a comprehensive set of endogenous oxylipins derived from LO conversion of LA, EPA, DHA and AA in HEK293T_LPCAT2_LO, (LO: 5-LO, 15-LO1 or 15-LO2) cells. LO expression was induced with doxycycline for 24 h followed by treatment with 10 µM RSL3, 1 µM Fer-1 or a combination of both for 4 h. Both non-esterified/free and total oxylipins were determined by LC-MS (Rund et al., 2018; Kutzner et al., 2019; Ostermann et al., 2020; Hartung et al., 2023). The obtained concentrations were normalized to total protein content and compared to DMSO controls. In HEK293T_LPCAT2 cells without LO expression, 13-HODE was the only oxylipin found non-esterified at low levels, all other oxylipins were fully esterified in the membrane. Neither RSL3 nor Fer-1 or RSL3/Fer-1 treatment had a significant effect on the concentration of oxylipins. In 5-LO expressing cells, there was no increase in the levels of 5-HETE, LTB_4, 5-HEPE and 4-HDHA. All 5-LO products were fully esterified and neither treatment resulted in an altered product spectrum. Interestingly, in HEK293T_LPCAT2_15LO1 cells, total concentrations of 13-HODE were elevated. RSL3 treatment significantly increased the total levels of 13-HODE and 15-HETE and also led to elevated levels of 12-HETE, 15-HEPE and 17-HDHA. Combined treatment with the ferroptosis inhibitor Fer-1 led to slightly decreased levels for all oxylipins. Again, 13-HODE was the only oxylipin that was found non-esterified in significant levels. HEK293T_LPCAT2_15LO2 cells also showed strongly elevated levels of 13-HODE, 15-HETE, 15-HEPE and 17-HDHA compared to HEK293T_LPCAT2 cells. Comparing the level of free 13-HODE with 15-LO1-overexpressing cells, it was decreased in 15-LO2-expressing cells. However, as with 5-LO overexpressing cells, RSL3 and Fer-1 treatment had no effect on the levels of the LO products.

In summary, 13-HODE was the only oxylipin that was non-esterified to some extent; all other LO products were almost completely esterified. Overexpression of 5-LO did not result in increased LO products, whereas overexpression of 15-LO1 and 15-LO2 did. Interestingly, RSL3 treatment had an effect only on 15-LO1 expressing cells, resulting in increased levels of all 15-LO1 products. Treatment with Fer-1 resulted in a slight inhibition of the RSL3 effect. It should be noted that the RLS3 treatment led to a relevant ferroptosis (see section 3.5) thus the change in oxylipin concentration may also arise from the cytotoxicity and not only from changes in lipids occurring in early ferroptosis.

4 Discussion

4.1 A link between LPCAT2 and ferroptosis

Macrophages are responsible for the maintenance of cell homeostasis. As part of the innate immune system, one purpose is to clear cellular debris including ferroptotic cells (Chen et al., 2021a) which can result in iron accumulation and thus an increased risk of developing ferroptosis in macrophages themselves. Interestingly, macrophages express high levels of LPCAT2 (Shindou et al., 2007), an isoenzyme of LPCAT3 which is usually studied in the field of ferroptosis. Thus, we first checked and confirmed a high protein expression of LPCAT2 in primary M1 and M2 macrophages. In order to investigate their influence

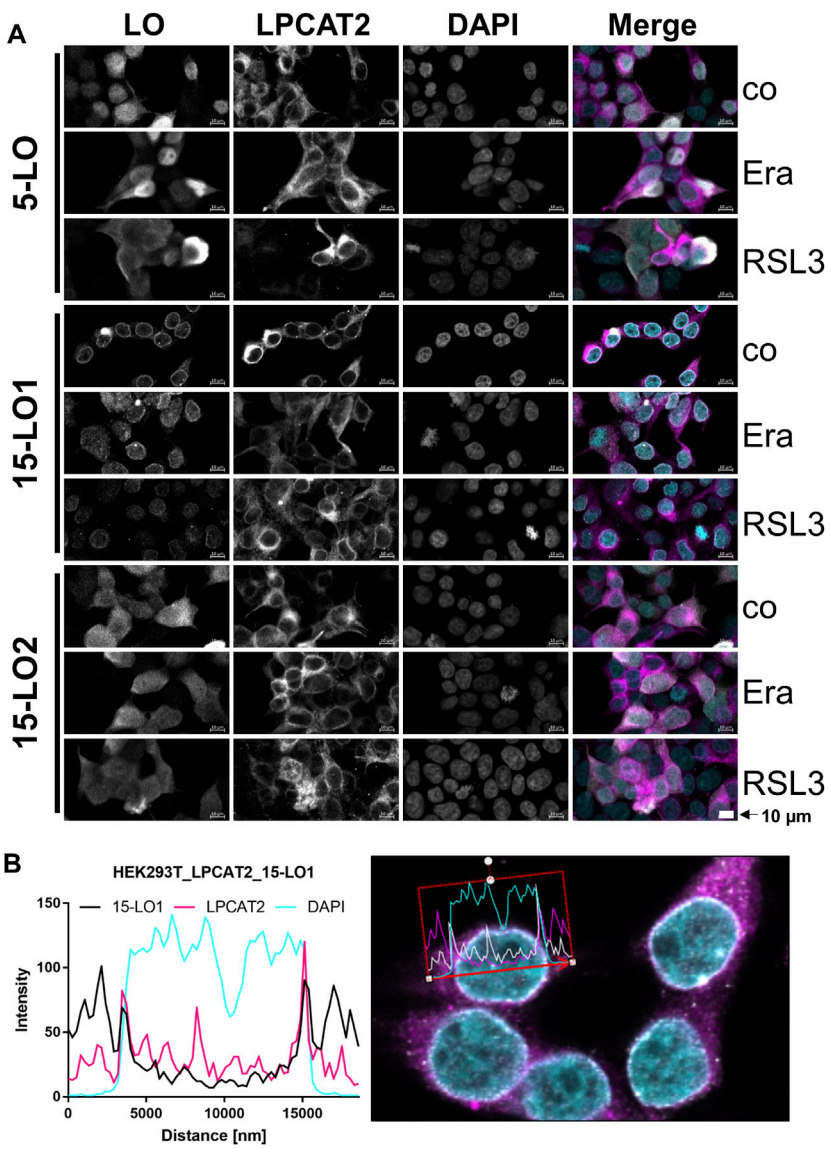

FIGURE 8
Localization of LOs in stably transfected HEK293T_LPCAT2 cells. HEK293T_LPCAT2_LO (LO: 5-LO, 15-LO1 or 15-LO2) cells were treated with 200 ng/mL doxycycline for 24 h before treatment with 10 µM RSL3 or 3 µM erastin (Era) for 4 or 24 h, respectively. Controls (co) received DMSO. Cells were stained with fluorophore-conjugated secondary antibodies against specific primary antibodies. Nuclei were counterstained using DAPI. Cells were imaged and analyzed on a Zeiss 780 AxioObserver.Z1 laser scanning confocal microscope (Carl Zeiss AG). **(A)** Images display a representative part of the acquired total image. Fluorescence of single channels is shown in black and white for better contrast, with the overlaid image shown in color (LOs: white; LPCAT2: purple, DAPI: turquoise). 10 µm scale bars are given in each image. Images display one of 3 independent experiments. **(B)** Histogram of fluorescence intensities (15-LO1: black, LPCAT2: purple, DAPI: turquoise) vs. distance (left) of a cellular profile (right, 15-LO1: white; LPCAT2: purple; DAPI: turquoise) of HEK293T_LPCAT2_15LO1 cells. Brightness and contrast were adjusted in a linear fashion.

on ferroptosis, we prepared HEK293T cells stably overexpressing LPCAT2 and/or ACSL4, an enzyme well known as biomarker and contributor of ferroptosis (Yuan et al., 2016). Treating the transfected cells with ferroptosis inducing agents resulted in an increased responsiveness to these compounds. Although HEK293T cells already express ACSL4 endogenously, a combination of both enzymes resulted in the strongest effects pointing out that the combination of ferroptosis inducing agents on one hand and ferroptosis enhancing enzymes on the other hand leads to a decrease in cell viability. This supports that LPCAT2, besides LPCAT3, is involved in the promotion of ferroptosis.

4.2 Lipoxygenase localization

Lipid peroxidation is a major requirement for ferroptotic cell death and is either caused by iron-mediated generation of ROS (Chen et al., 2020) or by iron-containing enzymes like lipoxygenases (LOs) (Chen et al., 2021a). Although expression of LOs is not mandatory for the development of ferroptosis, their presence was shown to sensitize cells to ferroptosis (Shah et al., 2018). Thus, we prepared an inducible overexpression system for 5-LO and 15-LO1/2 in our stably transfected HEK293T cells and investigated the localization of the LOs in native and ferroptotic state. Being a mobile

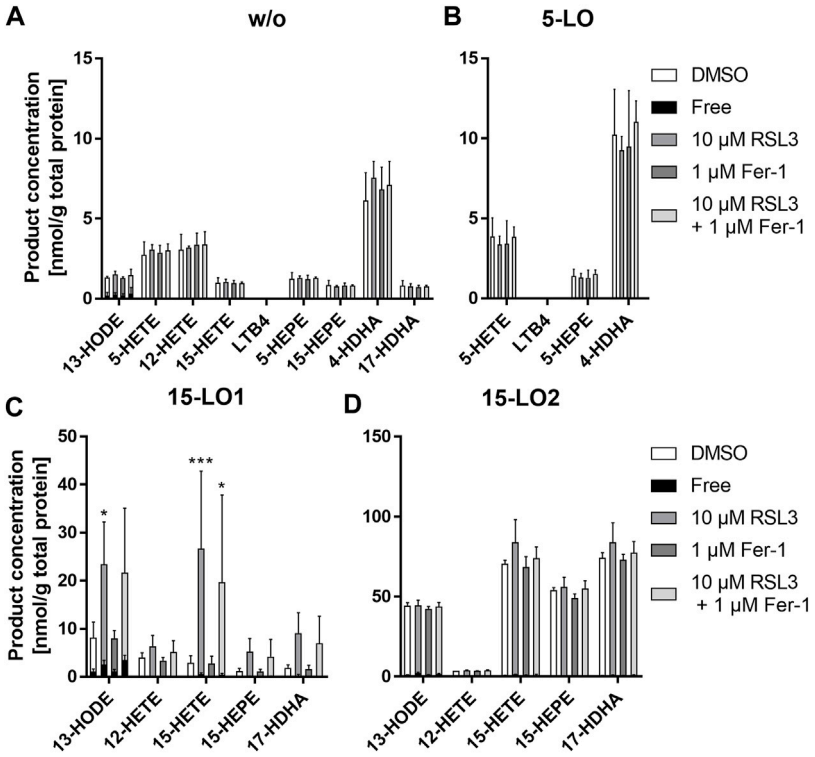

FIGURE 9
RSL3 treatment increases oxylipin formation in 15-LO1 expressing cells after 4 h. Levels of esterified and non-esterified oxylipins were determined in 1×10^7 HEK293_LPCAT2 **(A)** HEK293T_LPCAT2_5LO **(B)**, HEK293T_LPCAT2_15LO1 **(C)** or HEK293T_LPCAT2_15LO2 **(D)** cells. **(B–D)** were treated with 200 ng/mL doxycycline for 24 h prior to treatment with 10 µM RSL3, 1 µM Fer-1 or a combination of both for 4 h HEK293T_LPCAT2 cells **(A)** served as LO control and DMSO-treated cells served as compound controls. Free and total (free + esterified) oxylipin levels were determined via LC-MS as described and normalized on the total protein content of each sample. The inner black part of each bar represents the non-esterified proportion of the respective oxylipin. Data display mean +SD of 3 independent experiments. Statistical analysis was performed against DMSO controls and significance was tested using 2-way ANOVA with Dunnett's multiple comparisons test. Total oxylipins: $*p < 0.05$, $**p < 0.01$, $***p < 0.001$.

enzyme, 5-LO can reside in the cytosol as well as in the nucleus. Thereby, the localization depends largely on the cell type and activation state of the cells. Here, we found 5-LO nearly exclusively in the cytosolic region in untreated vector control cells (HEK293T_VC_5LO, Figure 7) what differs from previous reports that describe a localization within the nucleus of 5-LO overexpressing HEK293 cells (Häfner et al., 2015; Gilbert et al., 2020). One reason may be that we did not stimulate our cells with exogenous AA or calcium ionophore instead we performed our experiments under standard cultivation conditions. Second, this might be an effect of the different experimental setup, since most published data on the localization of 5-LO in HEK293T cells results from constitutively overexpressed 5-LO resulting in a stronger upregulation of 5-LO expression whereas, in our setup, 5-LO is inducible and therefore only present for a short time period. This may result in fewer cellular stress by oxylipins and thus less activation of p38 followed by lower phosphorylation of Ser271 (Harrison and Murphy, 1995; Cho et al., 2011). As published previously, 5-LO is localized in the nucleus in HEK293T cells stably overexpressing GFP-5-LO, which can be shifted to the cytosol by Ser271Ala mutation in combination with CaMKII inhibitor KN-93 and the p38 inhibitor SB203580 (Ball et al., 2017). Thus, enhanced phosphorylation could explain the shift from cellular to nuclear localization of 5-LO following treatment with ferroptosis inducing agents RSL3 and erastin in our HEK293T_VC cells (Figure 7). In addition, we see a similar behavior of 15-LO1 which accumulates at the nuclear envelope after RSL3 treatment and 15-LO2, which shows localization all over the cell after treatment with RSL3 or erastin in HEK293T_VC cells. Interestingly, the same change in cellular localization for each LO was visible in cells overexpressing the LPCAT2 gene (Figure 8) even without RSL3 or erastin treatment. Since LPCAT2 expression shows the same effect as treatment with ferroptosis inducing agents, the enzyme seems to cause ferroptotic conditions itself indicating that LPCAT2 might be a target worth investigating in future studies.

4.3 Oxylipin formation

When we investigated the basal oxylipin formation without treatment in our HEK293T_LPCAT2 cells, LO products were almost completely esterified. Following LO expression in HEK293T_LPCAT2_LO cells we obtained no change in 5-LO product levels, while 15-LO1 and 15-LO2 products were detected at high concentrations mostly esterified. Only 13-HODE and low amounts of 15-HETE were detected non-esterified. This could be

caused by the cellular localization of the LOs. Activation of 5-LO is triggered by increases in intracellular calcium and phosphorylation causing co-localization with cytosolic phospholipase A_2 (cPLA) at the nuclear envelope. $cPLA_2$ releases AA from the membrane which is then transferred by the 5-lipoxygenase-activating protein (FLAP) into the active site of 5-LO (Peters-Golden and Brock, 2001; Evans et al., 2008). Previous studies already showed that 5-LO overexpressing HEK293 cells lack 5-LO activity in the absence of exogenously added AA (Gerstmeier et al., 2014). Since we do not have FLAP in our system this may result in fewer basal products.

15-LO1 and 15-LO2 stand out from other LOs since they are able to convert both free and membrane-bound PUFAs (Snodgrass and Brüne, 2019). Interestingly, we found that 15-LO1 is located directly at the nuclear envelope and therefore may have direct access to its substrates at the membrane (Figure 7). Since only 15-LO1 expressing cells show elevated products levels after RSL3 treatment, location of the LO at the nuclear membrane seems to be important. Surprisingly, additional treatment of the cells with the ferroptosis inhibitor Fer-1 only slightly inhibited this effect. Because Fer-1 acts as a radical scavenging antioxidant and does not directly inhibit 15-LO1 (Zilka et al., 2017), the enzyme appears to convert oxylipins directly at the membrane, where they can be rapidly incorporated. Although 15-LO2 is not located at the nuclear membrane, its product levels increased after induction of LO expression, suggesting that the localization of the LO is not as important for increased product formation as for the product formation after RSL3 treatment. Our LO localization study revealed that RSL3 treatment of HEK293T_VC_15-LO1 cells causes a 15-LO1 localization at the nuclear membrane which was not observed with erastin treatment (Figure 7). Interestingly, 15-LO1 was already present at the nuclear envelope in untreated HEK293T_LPCAT2_15-LO1 cells indicating that LPCAT2 overexpression might affect 15-LO1 localization in a similar way as RSL3 does. In contrast to erastin which inhibits GPX4 by GSH depletion, RSL3 inactivates GPX4 directly and thereby inhibits its antioxidative function (Yang et al., 2014). Translocation of 15-LO1 to the nuclear membrane to form a complex with the phosphatidylethanolamine binding protein 1 (PEBP1) has been reported to act as redox assembly in combination with GPX4 as antagonist (Wenzel et al., 2017). This complex then leads to the formation of esterified oxylipins such as 15-HpETE-PE which promote ferroptosis if GPX4 is impaired. Furthermore, PEBP1 is described to cause enhanced sensitivity to ferroptosis by RSL3 treatment in kidney cells. Because our data indicate that the presence of LPCAT2 has a similar effect as RSL3 treatment on the localization of 15-LO1 and both enzymes are present around the nuclear membrane in spatial proximity (Figure 8B), it will be interesting to see whether future studies may demonstrate a PEBP1-like interaction of these enzymes.

4.4 Conclusion

Here, we report for the first time that not only LPCAT3 but also LPCAT2 may be involved in the iron-dependent cell death mechanism known as ferroptosis. When it comes to the investigation of cell death mechanisms, it is usually complicated to distinguish between multiple causes. Therefore, our smart cell-based model system allows the precise activation of lipoxygenase-mediated lipid peroxidation, which enables experimental setups to study ferroptotic effects in detail. Future studies might include the investigation of effects of varying enzyme expression levels, the manipulation of oxylipin formation with both endogenous and exogenous substrates as well as more detailed studies on the effect of ferroptosis induction by erastin.

Data availability statement

The original contributions presented in the study are included in the article/Supplementary Material, further inquiries can be directed to the corresponding authors.

Ethics statement

Ethical approval was not required for the studies on humans in accordance with the local legislation and institutional requirements because only commercially available established cell lines were used.

Author contributions

BG: conceptualization, methodology, writing–original draft, formal analysis, and project administration. LC: methodology, investigation, and formal analysis. SR: methodology, investigation, and formal analysis. TG: methodology and investigation. SS: investigation. NS: conceptualization, resources, supervision, writing–review and editing, and funding acquisition. DS: conceptualization, resources, supervision, writing–review and editing, and funding acquisition. A-KH: conceptualization, writing–original draft, supervision, and writing–review and editing. All authors contributed to the article and approved the submitted version.

Funding

Work of the authors was supported by the Deutsche Forschungsgemeinschaft (SFB 1039 TP A02, GRK 2336 TP4, SCHE1801).

Acknowledgments

The authors thank Marcel Müller for providing macrophage cell lysates. Figure 3 was created with BioRender.com.

Conflict of interest

The authors declare that the research was conducted in the absence of any commercial or financial relationships that could be construed as a potential conflict of interest.

The author DS declared that they were an editorial board member of Frontiers, at the time of submission. This had no impact on the peer review process and the final decision.

Publisher's note

All claims expressed in this article are solely those of the authors and do not necessarily represent those of their affiliated organizations, or those of the publisher, the editors and the reviewers. Any product that may be evaluated in this article, or claim that may be made by its manufacturer, is not guaranteed or endorsed by the publisher.

Supplementary material

The Supplementary Material for this article can be found online at: https://www.frontiersin.org/articles/10.3389/fceld.2023.1182239/full#supplementary-material

References

Abate, W., Alrammah, H., Kiernan, M., Tonks, A. J., and Jackson, S. K. (2020). Lysophosphatidylcholine acyltransferase 2 (LPCAT2) co-localises with TLR4 and regulates macrophage inflammatory gene expression in response to LPS. *Sci. Rep.* 10, 10355–10413. doi:10.1038/s41598-020-67000-x

Agarwal, A. K., and Garg, A. (2010). Enzymatic activity of the human 1-acylglycerol-3-phosphate-O-acyltransferase isoform 11: upregulated in breast and cervical cancers. *J. Lipid Res.* 51, 2143–2152. doi:10.1194/jlr.M004762

Amaral, E. P., Costa, D. L., Namasivayam, S., Riteau, N., Kamenyeva, O., Mittereder, L., et al. (2019). A major role for ferroptosis in Mycobacterium tuberculosis–induced cell death and tissue necrosis. *J. Exp. Med.* 216, 556–570. doi:10.1084/jem.20181776

Ansari, I. H., Longacre, M. J., Stoker, S. W., Kendrick, M. A., O'Neill, L. M., Zitur, L. J., et al. (2017). Characterization of Acyl-CoA synthetase isoforms in pancreatic beta cells: gene silencing shows participation of ACSL3 and ACSL4 in insulin secretion. *Arch. Biochem. Biophys.* 618, 32–43. doi:10.1016/j.abb.2017.02.001

Ball, A. -K., Beilstein, K., Wittmann, S., Sürün, D., Saul, M. J., Schnütgen, F., et al. (2017). Characterization and cellular localization of human 5-lipoxygenase and its protein isoforms 5-LOp13, 5-LOp4 and 5-LOp12. *Biochim. Biophys. Acta—Mol. Cell Biol. Lipids* 1862, 561–571. doi:10.1016/j.bbalip.2017.02.015

Chen, X., Kang, R., Kroemer, G., and Tang, D. (2021a). Ferroptosis in infection, inflammation, and immunity. *J. Exp. Med.* 218, e20210518. doi:10.1084/jem.20210518

Chen, X., Kang, R., and Tang, D. (2021b). Ferroptosis by lipid peroxidation: the tip of the iceberg? *Front. Cell Dev. Biol.* 9, 646890. doi:10.3389/fcell.2021.646890

Chen, X., Yu, C., Kang, R., and Tang, D. (2020). Iron metabolism in ferroptosis. *Front. Cell Dev. Biol.* 8, 590226. doi:10.3389/fcell.2020.590226

Cho, K.-J., Seo, J.-M., and Kim, J.-H. (2011). Bioactive lipoxygenase metabolites stimulation of NADPH oxidases and reactive oxygen species. *Mol. Cells* 32, 1–5. doi:10.1007/s10059-011-1021-7

Chu, B., Kon, N., Chen, D., Li, T., Liu, T., Jiang, L., et al. (2019). ALOX12 is required for p53-mediated tumour suppression through a distinct ferroptosis pathway. *Nat. Cell Biol.* 21, 579–591. doi:10.1038/s41556-019-0305-6

Dar, H. H., Tyurina, Y. Y., Mikulska-Ruminska, K., Shrivastava, I., Ting, H.-C., Tyurin, V. A., et al. (2018). Pseudomonas aeruginosa utilizes host polyunsaturated phosphatidylethanolamines to trigger theft-ferroptosis in bronchial epithelium. *J. Clin. Invest.* 128, 4639–4653. doi:10.1172/JCI99490

Dixon, S. J., Lemberg, K. M., Lamprecht, M. R., Skouta, R., Zaitsev, E. M., Gleason, C. E., et al. (2012). Ferroptosis: an iron-dependent form of nonapoptotic cell death. *Cell* 149, 1060–1072. doi:10.1016/j.cell.2012.03.042

Dixon, S. J., Winter, G. E., Musavi, L. S., Lee, E. D., Snijder, B., Rebsamen, M., et al. (2015). Human haploid cell genetics reveals roles for lipid metabolism genes in nonapoptotic cell death. *ACS Chem. Biol.* 10, 1604–1609. doi:10.1021/acschembio.5b00245

Doll, S., Proneth, B., Tyurina, Y. Y., Panzilius, E., Kobayashi, S., Ingold, I., et al. (2017). ACSL4 dictates ferroptosis sensitivity by shaping cellular lipid composition. *Nat. Chem. Biol.* 13, 91–98. doi:10.1038/nchembio.2239

Ebert, R., Cumbana, R., Lehmann, C., Kutzner, L., Toewe, A., Ferreirós, N., et al. (2020). Long-term stimulation of toll-like receptor-2 and -4 upregulates 5-LO and 15-LO-2 expression thereby inducing a lipid mediator shift in human monocyte-derived macrophages. *Biochim. Biophys. Acta - Mol. Cell Biol. Lipids* 1865, 158702. doi:10.1016/j.bbalip.2020.158702

Evans, J. F., Ferguson, A. D., Mosley, R. T., and Hutchinson, J. H. (2008). What's all the FLAP about? 5-lipoxygenase-activating protein inhibitors for inflammatory diseases. *Trends Pharmacol. Sci.* 29, 72–78. doi:10.1016/j.tips.2007.11.006

Gerstmeier, J., Weinigel, C., Barz, D., Werz, O., and Garscha, U. (2014). An experimental cell-based model for studying the cell biology and molecular pharmacology of 5-lipoxygenase-activating protein in leukotriene biosynthesis. *Biochim. Biophys. Acta - Gen. Subj.* 1840, 2961–2969. doi:10.1016/j.bbagen.2014.05.016

Gilbert, N. C., Gerstmeier, J., Schexnaydre, E. E., Börner, F., Garscha, U., Neau, D. B., et al. (2020). Structural and mechanistic insights into 5-lipoxygenase inhibition by natural products. *Nat. Chem. Biol.* 16, 783–790. doi:10.1038/s41589-020-0544-7

Häfner, A. K., Gerstmeier, J., Hörnig, M., George, S., Ball, A. K., Schröder, M., et al. (2015). Characterization of the interaction of human 5-lipoxygenase with its activating protein FLAP. *Biochim. Biophys. Acta - Mol. Cell Biol. Lipids* 1851, 1465–1472. doi:10.1016/j.bbalip.2015.08.010

Han, F., Li, S., Yang, Y., and Bai, Z. (2021). Interleukin-6 promotes ferroptosis in bronchial epithelial cells by inducing reactive oxygen species-dependent lipid peroxidation and disrupting iron homeostasis. *Bioengineered* 12, 5279–5288. doi:10.1080/21655979.2021.1964158

Harrison, K. A., and Murphy, R. C. (1995). Isoleukotrienes are biologically active free radical products of lipid peroxidation. *J. Biol. Chem.* 270, 17273–17278. doi:10.1074/jbc.270.29.17273

Hartung, N. M., Mainka, M., Pfaff, R., Kuhn, M., Biernacki, S., Zinnert, L., et al. (2023). Development of a quantitative proteomics approach for cyclooxygenases and lipoxygenases in parallel to quantitative oxylipin analysis allowing the comprehensive investigation of the arachidonic acid cascade. *Anal. Bioanal. Chem.* 415, 913–933. doi:10.1007/s00216-022-04489-3

Jiang, L., Kon, N., Li, T., Wang, S.-J., Su, T., Hibshoosh, H., et al. (2015). Ferroptosis as a p53-mediated activity during tumour suppression. *Nature* 520, 57–62. doi:10.1038/nature14344

Kang, M.-J., Fujino, T., Sasano, H., Minekura, H., Yabuki, N., Nagura, H., et al. (1997). A novel arachidonate-preferring acyl-CoA synthetase is present in steroidogenic cells of the rat adrenal, ovary, and testis. *Proc. Natl. Acad. Sci. U.S.A.* 94, 2880–2884. doi:10.1073/pnas.94.7.2880

Kowarz, E., Löscher, D., and Marschalek, R. (2015). Optimized sleeping beauty transposons rapidly generate stable transgenic cell lines. *Biotechnol. J.* 10, 647–653. doi:10.1002/biot.201400821

Kreiß, M., Oberlis, J. H., Seuter, S., Bischoff-Kont, I., Sürün, D., Thomas, D., et al. (2022). Human 5-lipoxygenase regulates transcription by association to euchromatin. *Biochem. Pharmacol.* 203, 115187. doi:10.1016/j.bcp.2022.115187

Kuang, F., Liu, J., Xie, Y., Tang, D., and Kang, R. (2021). MGST1 is a redox-sensitive repressor of ferroptosis in pancreatic cancer cells. *Cell Chem. Biol.* 28, 765–775.e5. doi:10.1016/j.chembiol.2021.01.006

Küch, E.-M., Vellaramkalayil, R., Zhang, I., Lehnen, D., Brügger, B., Stremmel, W., et al. (2014). Differentially localized acyl-CoA synthetase 4 isoenzymes mediate the metabolic channeling of fatty acids towards phosphatidylinositol. *Biochim. Biophys. Acta - Mol. Cell Biol. Lipids* 1841, 227–239. doi:10.1016/j.bbalip.2013.10.018

Kutzner, L., Rund, K. M., Ostermann, A. I., Hartung, N. M., Galano, J.-M., Balas, L., et al. (2019). Development of an optimized LC-MS method for the detection of specialized pro-resolving mediators in biological samples. *Front. Pharmacol.* 10, 169. doi:10.3389/fphar.2019.00169

Lai, B., Wu, C.-H., Wu, C.-Y., Luo, S.-F., and Lai, J.-H. (2022). Ferroptosis and autoimmune diseases. *Front. Immunol.* 13, 916664. doi:10.3389/fimmu.2022.916664

Lands, W. E. (1958). Metabolism of glycerolipides; a comparison of lecithin and triglyceride synthesis. *J. Biol. Chem.* 231, 883–888. doi:10.1016/S0021-9258(18)70453-5

Lands, W. E. M., and Merkl, I. (1963). Metabolism of glycerolipids. *J. Biol. Chem.* 238, 898–904. doi:10.1016/S0021-9258(18)81234-0

Lewin, T. M., Kim, J.-H., Granger, D. A., Vance, J. E., and Coleman, R. A. (2001). Acyl-CoA synthetase isoforms 1, 4, and 5 are present in different subcellular membranes in rat liver and can be inhibited independently. *J. Biol. Chem.* 276, 24674–24679. doi:10.1074/jbc.M102036200

Li, C., Zhang, Y., Liu, J., Kang, R., Klionsky, D. J., and Tang, D. (2021). Mitochondrial DNA stress triggers autophagy-dependent ferroptotic death. *Autophagy* 17, 948–960. doi:10.1080/15548627.2020.1739447

Liu, Z., Huang, Y., Hu, W., Huang, S., Wang, Q., Han, J., et al. (2014). dAcsl, the drosophila ortholog of Acyl-CoA synthetase long-chain family Member 3 and 4, inhibits synapse growth by attenuating bone morphogenetic protein signaling via endocytic recycling. *J. Neurosci.* 34, 2785–2796. doi:10.1523/JNEUROSCI.3547-13.2014

Luo, X., Gong, H.-B., Gao, H.-Y., Wu, Y.-P., Sun, W.-Y., Li, Z.-Q., et al. (2021). Oxygenated phosphatidylethanolamine navigates phagocytosis of ferroptotic cells by interacting with TLR2. *Cell Death Differ.* 28, 1971–1989. doi:10.1038/s41418-020-00719-2

Ostermann, A. I., Koch, E., Rund, K. M., Kutzner, L., Mainka, M., and Schebb, N. H. (2020). Targeting esterified oxylipins by LC-MS - effect of sample preparation on oxylipin pattern. *Prostagl. Other Lipid Mediat* 146, 106384. doi:10.1016/j.prostaglandins.2019.106384

Peters-Golden, M., and Brock, T. G. (2001). Intracellular compartmentalization of leukotriene synthesis: unexpected nuclear secrets. *FEBS Lett.* 487, 323–326. doi:10.1016/s0014-5793(00)02374-7

Rund, K. M., Ostermann, A. I., Kutzner, L., Galano, J.-M., Oger, C., Vigor, C., et al. (2018). Development of an LC-ESI(-)-MS/MS method for the simultaneous quantification of 35 isoprostanes and isofurans derived from the major n3-and n6-PUFAs. *Anal. Chim. Acta* 1037, 63–74. doi:10.1016/j.aca.2017.11.002

Shah, R., Shchepinov, M. S., and Pratt, D. A. (2018). Resolving the role of lipoxygenases in the initiation and execution of ferroptosis. *ACS Cent. Sci.* 4, 387–396. doi:10.1021/acscentsci.7b00589

Shindou, H., Hishikawa, D., Nakanishi, H., Harayama, T., Ishii, S., Taguchi, R., et al. (2007). A single enzyme catalyzes both platelet-activating factor production and membrane biogenesis of inflammatory cells. Cloning and characterization of acetyl-CoA:LYSO-PAF acetyltransferase. *J. Biol. Chem.* 282, 6532–6539. doi:10.1074/jbc.M609641200

Snodgrass, R. G., and Brüne, B. (2019). Regulation and functions of 15-lipoxygenases in human macrophages. *Front. Pharmacol.* 10, 719. doi:10.3389/fphar.2019.00719

Soupene, E., Fyrst, H., and Kuypers, F. A. (2008). Mammalian acyl-CoA: lysophosphatidylcholine acyltransferase enzymes. *Proc. Natl. Acad. Sci. U.S.A.* 105, 88–93. doi:10.1073/pnas.0709737104

Stockwell, B. R. (2022). Ferroptosis turns 10: emerging mechanisms, physiological functions, and therapeutic applications. *Cell* 185, 2401–2421. doi:10.1016/j.cell.2022.06.003

Upton, J. E. M., Grunebaum, E., Sussman, G., and Vadas, P. (2022). Platelet activating factor (PAF): a mediator of inflammation. *BioFactors* 48, 1189–1202. doi:10.1002/biof.1883

Wang, B., and Tontonoz, P. (2019). Phospholipid remodeling in physiology and disease. *Annu. Rev. Physiol.* 81, 165–188. doi:10.1146/annurev-physiol-020518-114444

Wang, H., An, P., Xie, E., Wu, Q., Fang, X., Gao, H., et al. (2017). Characterization of ferroptosis in murine models of hemochromatosis. *Hepatology* 66, 449–465. doi:10.1002/hep.29117

Wenzel, S. E., Tyurina, Y. Y., Zhao, J., Croix, M. S. C., Dar, H. H., Mao, G., et al. (2017). PEBP1 wardens ferroptosis by enabling lipoxygenase generation of lipid death signals. *Cell* 171, 628–641. doi:10.1016/j.cell.2017.09.044

Werz, O., and Steinhilber, D. (1996). Selenium-dependent peroxidases suppress 5-lipoxygenase activity in B-lymphocytes and immature myeloid cells. The presence of peroxidase-insensitive 5-lipoxygenase activity in differentiated myeloid cells. *Eur. J. Biochem.* 242, 90–97. doi:10.1111/j.1432-1033.1996.0090r.x

Yan, B., Ai, Y., Sun, Q., Ma, Y., Cao, Y., Wang, J., et al. (2021). Membrane damage during ferroptosis is caused by oxidation of phospholipids catalyzed by the oxidoreductases POR and CYB5R1. *Mol. Cell* 81, 355–369. doi:10.1016/j.molcel.2020.11.024

Yamane, D., Hayashi, Y., Matsumoto, M., Nakanishi, H., Imagawa, H., Kohara, M., et al. (2022). FADS2-dependent fatty acid desaturation dictates cellular sensitivity to ferroptosis and permissiveness for hepatitis C virus replication. *Cell Chem. Biol.* 29, 799–810.e4. doi:10.1016/j.chembiol.2021.07.022

Yamashita, A., Hayashi, Y., Nemoto-Sasaki, Y., Ito, M., Oka, S., Tanikawa, T., et al. (2014). Acyltransferases and transacylases that determine the fatty acid composition of glycerolipids and the metabolism of bioactive lipid mediators in mammalian cells and model organisms. *Prog. Lipid Res.* 53, 18–81. doi:10.1016/j.plipres.2013.10.001

Yang, W. S., Kim, K. J., Gaschler, M. M., Patel, M., Shchepinov, M. S., and Stockwell, B. R. (2016). Peroxidation of polyunsaturated fatty acids by lipoxygenases drives ferroptosis. *Proc. Natl. Acad. Sci. U.S.A.* 113, E4966–E4975. doi:10.1073/pnas.1603244113

Yang, W. S., Sriramaratnam, R., Welsch, M. E., Shimada, K., Skouta, R., Viswanathan, V. S., et al. (2014). Regulation of ferroptotic cancer cell death by GPX4. *Cell* 156, 317–331. doi:10.1016/j.cell.2013.12.010

Yuan, H., Li, X., Zhang, X., Kang, R., and Tang, D. (2016). Identification of ACSL4 as a biomarker and contributor of ferroptosis. *Biochem. Biophys. Res. Commun.* 478, 1338–1343. doi:10.1016/j.bbrc.2016.08.124

Zilka, O., Shah, R., Li, B., Friedmann Angeli, J. P., Griesser, M., Conrad, M., et al. (2017). On the mechanism of cytoprotection by ferrostatin-1 and liproxstatin-1 and the role of lipid peroxidation in ferroptotic cell death. *ACS Cent. Sci.* 3, 232–243. doi:10.1021/acscentsci.7b00028

Zou, Y., Li, H., Graham, E. T., Deik, A. A., Eaton, J. K., Wang, W., et al. (2020). Cytochrome P450 oxidoreductase contributes to phospholipid peroxidation in ferroptosis. *Nat. Chem. Biol.* 16, 302–309. doi:10.1038/s41589-020-0472-6